Electronic structure of $EuCu_2Ge_2$ studied by resonant photoemission and x-ray absorption spectroscopy

Soma Banik,[1,*] Azzedine Bendounan,[2] A. Thamizhavel,[3] A. Arya,[4] P. Risterucci,[2] F. Sirotti,[2] A. K. Sinha,[1] S. K. Dhar,[3] and S. K. Deb[1]

[1]*Indus Synchrotron Utilization Division, Raja Ramanna Centre for Advanced Technology, Indore 452013, India*
[2]*Synchrotron SOLEIL, L'Orme des Merisiers, Saint-Aubin, BP 48, FR-91192 Gif-sur-Yvette Cedex, France*
[3]*Tata Institute of Fundamental Research, Homi Bhabha Road, Colaba, Mumbai 400005, India*
[4]*Materials Science Division, Bhabha Atomic Research Centre, Mumbai 400085, India*

(Received 18 February 2012; published 23 August 2012)

The electronic structure of $EuCu_2Ge_2$ single crystal has been investigated by the valence band photoemission across the Eu $4d$-$4f$ resonance and Eu L_3 x-ray absorption edge spectroscopy. Signatures of both the Eu^{2+} and Eu^{3+} states are observed in the resonant photoemission near the $4d$ threshold of Eu at 140 and 143 eV, respectively. The constant initial state spectra for Eu^{2+} and Eu^{3+} states exhibit Fano-type resonance profile. The experimental spectra have been interpreted with the help of first-principles density functional calculations within the generalized gradient approximations taking into account the strong intra-atomic (*onsite*) interaction Hubbard U term. The Eu $4f$ related resonant features are found to be hybridized with the Cu and Ge states. Supporting evidence for the existence of Eu in Eu^{2+} (92%) and Eu^{3+} (8%) states are also obtained from the x-ray absorption edge spectra, which probe the bulk response. Both the resonant photoemission and Eu L_3 x-ray absorption edge spectroscopy gives the evidence that Eu is present in the inhomogeneous and static mixed valence state in $EuCu_2Ge_2$.

DOI: 10.1103/PhysRevB.86.085134 PACS number(s): 79.60.−i, 71.20.Eh, 71.27.+a

I. INTRODUCTION

Europium intermetallic compounds of the type EuM_2X_2, where M is a transition metal and X is silicon or germanium, belongs to a wide group of compounds, some of which exhibit mixed or unstable valence of europium. For example, europium valence in polycrystalline $EuCu_2Si_2$ and $EuPd_2Si_2$ fluctuates and changes with temperature and in $EuNi_2Ge_2$, it changes with applied pressure.[1–3] The integral valence state of europium in solids can be either divalent and magnetic (Eu^{2+};$4f^7$), or trivalent and nonmagnetic (Eu^{3+};$4f^6$). In homogeneous mixed valence Eu compounds, the f electrons are itinerant with dynamical fluctuations between $4f^6$ and $4f^7$, whereas in inhomogeneous mixed valence Eu compounds a static distribution of Eu^{2+} and Eu^{3+} is observed. During the last several decades, the mixed-valence phenomenon has attracted a great deal of interest in connection with valence fluctuations in these Eu based systems.[1–3]

$EuCu_2Ge_2$ belongs to a family of strongly correlated systems. $EuCu_2Ge_2$ shows a paramagnetic phase at room temperature and undergoes two antiferromagnetic transitions at 5.3 and 8.2 K.[4] From ^{151}Eu Mössbauer spectroscopy, $EuCu_2Ge_2$ is reported to have a stable divalent configuration in the temperature range from 2–300 K.[4,5] The stability of divalent Eu state in $EuCu_2Ge_2$ is also shown by other bulk measurements like x-ray diffraction, magnetic susceptibility, thermopower, resistivity, specific heat, etc.[4] Recently, x-ray absorption spectroscopy (XAS) measurement has shown the presence of small amount of trivalent Eu state in this system, but no explanation has been given as to its origin.[6] Moreover, it has also been observed that the slight change in the composition or with Si doping in $EuCu_2Ge_2$ can alter the valence of Eu ions and mixed valence states have been observed.[6,7] So there is a controversy about the true valance state of Eu in $EuCu_2Ge_2$ as observed using different experimental techniques and it is necessary to examine these findings using other independent techniques. Similar kind of discrepancy from different measurement techniques has also been reported for various other Eu related systems. For example, $EuPd_2P_2$ the Mössbauer data showed only the divalent state, while the XAS measurement showed the mixed valence nature which was attributed to the partly extended $4f$ radius.[8] Mixed valence state has also been reported for $Eu_{0.83}Fe_4Sb_{12}$ from XAS measurement but stable divalent state has been observed from the Mössbauer measurement and attributed due to the shake-up effects and the presence of different local environments of Eu ions.[9] $EuRh_2P_2$ showed the similar behavior from Mössbauer and Eu L_3-edge absorption spectra and the mixed valence states has been attributed to hybridization of the Eu $4f$ states with the conduction band and the possibility of covalent Eu-P bonds in the system.[10] Thus it is evident that discrepancy in the valence state of Eu have been observed in many of the Eu based intermetallic alloys as determined from different experimental techniques. As the mixed valance state arise because of two $4f$ shell configurations namely $4f^n$ and $4f^{n-1}$, which have nearly degenerate energies, it is of interest to study the electronic states of $EuCu_2Ge_2$ to resolve the controversy arising due to XAS and Mössbauer measurements.

The origin of magnetism in the Eu based intermetallic systems has been reported to arise from the subtle interplay between the $4f$ electrons and the conduction electrons. It is reported that the $4f$ electrons interact with the conduction electrons, thus modifying the electronic structure in the vicinity of the Fermi energy which is responsible for the different valence state in this system. For a divalent compound like EuAuAs, the $4f$ states are well below the Fermi level E_F.[11] For a homogeneously mixed valence system, a small density of states related to Eu $4f$ is expected in the vicinity of

the E_F as in EuPdP.[11] But for static mixed valence compounds, no Eu $4f$ states are expected in the vicinity of E_F. So the degree of the overlap between $4f$ states and the conduction bands, or the degree of hybridization, decisively influences the properties of these Eu based intermetallic systems. Hence it is necessary to understand the electronic structure and to determine the valence state of $EuCu_2Ge_2$ to have a deeper knowledge about the correlation and the origin of magnetism in these systems. To probe the $4f$ levels at the particular threshold energy, resonant photoemission spectroscopy (RPES) has emerged as a very powerful tool. Hence, in this work, we have studied the electronic structure of $EuCu_2Ge_2$ by RPES across the $4d$-$4f$ resonance and x-ray absorption at Eu L_3 edge in order to understand the origin of strong correlation and magnetism in this system and to resolve the controversy about the Eu valence states determined from different measurement techniques.

II. METHODOLOGY

$EuCu_2Ge_2$ single crystal was grown by the self-flux method, taking advantage of the eutectic composition of Cu:Ge and using it as flux. The single crystals have been characterized by x-ray diffraction (XRD), magnetic susceptibility, heat capacity, and x-ray absorption spectroscopy (XAS). Both XRD and XAS measurements were performed at the angle-dispersive x-ray diffraction beamline (BL-12) on Indus-2 synchrotron radiation source, India. A high spectral resolution of about 1.5 eV at 10 keV was achieved using Si(311)-based double crystal monochromator.[12] Powder XRD of $EuCu_2Ge_2$ single crystal was recorded using Image plate Mar-345 detector. FIT2D software was used to generate the XRD pattern from the diffraction rings as obtained by Image plate data. XAS measurement was performed in the flurosence mode at the Eu L_3 edge in the energy range from 6940 to 7020 eV. The magnetic susceptibility along the two principal crystallographic directions was measured in an applied field of 3 KOe, in the temperature range from 1.8 to 300 K by using a Quantum Design superconducting quantum interference device (SQUID) magnetometer. The sample was initially cooled down to 1.8 K in zero applied field and then a magnetic field of 3 KOe was applied and the data were collected while warming up. The heat capacity measurement was performed using a Quantum Design physical properties measurement system in the temperature range from 1 to 20 K.

Preliminary RPES measurements on this sample was performed at the AIPES beamline on Indus-1 synchrotron radiation source, India with 400 meV resolution and the results are reported in Ref. 13. In this paper we present the high resolution RPES measurements which were performed at the high resolution photoelectron spectroscopy station of TEMPO beamline at Synchrotron SOLEIL, France.[14] To obtain atomically clean surface, the $EuCu_2Ge_2$ single crystals were cleaved *in situ* in a base pressure of 9×10^{-11} mbar and at a temperature of about 40 K. The data were recorded with a Scienta SES 2002 electron energy analyzer in transmission mode with the sample kept at about 40 K in ultrahigh vacuum and 20 meV resolution. The valence band (VB) spectra were measured as function of the photon energy from 134 to 170 eV using linear-polarized light.

Ab initio spin-polarized electronic structure calculations were performed within the density-functional theory (DFT)[15] using very accurate full-potential linearized augmented plane-wave (FP-LAPW) approach incorporating the spin-orbit (SO) coupling as implemented in WIEN2K code.[16] This is an implementation of a FP-LAPW plus local orbitals (LAPW + lo) method.[17] The APW + lo method expands the Kohn-Sham orbitals in atomic-like orbitals inside the atomic muffin-tin (MT) spheres and plane waves in the interstitial region. The details of the methods have been described elsewhere.[17,18] The Perdew, Burke, Ernzerhof (PBE)[19] gradient corrected local spin density approximation (LSDA-GGA) for the exchange correlation (XC) potential was used. The core shell states were treated within the relativistic DFT formalism. For the valence and local orbital states, the scalar relativistic DFT was used neglecting the SO interaction. The SO interaction was treated by the second-variational approach.[17,18] A plane-wave expansion with $R_{MT} \times K_{MAX}$ equal to nine was used and the dependence of the total energy on the number of k points in the irreducible wedge of the first Brillouin zone was explored within the linearized tetrahedron scheme by performing the calculation for 159 k points ($12 \times 12 \times 12$ mesh). The MT radii used for the calculations were 2.9, 2.4, and 2.1 Bohr for Eu, Cu, and Ge, respectively. To account for the Coulomb correlation interaction within the Eu-$4f$ shell, we additionally considered the PBE XC potential corrected according to GGA + U method. For Eu, the values of U and J parameters were taken to be 7.4 and 1.1 eV, respectively.[20] The total energy was minimized as a function of lattice parameters (a and c/a) and atomic position optimization was performed such that the residual force on each atom was less than 1 meV/Å. All ionic relaxations were performed by keeping the unit cell shape and volume fixed to that of the equilibrium bulk structure as predicted at the GGA level. The equilibrium lattice parameter was calculated to be $a = 4.168$ Å with $c/a = 2.451$ which agrees well with our experimental value of $a = 4.2117$ Å (and $c/a = 2.4274$) discussed later. The relaxed ionic positions for Eu:(0,0,0); Cu:(0,0.5,0.25); and Ge:(0,0,0.378) matched closely with experimental values of Eu:(0,0,0); Cu:(0,0.5,0.25); and Ge:(0,0,0.376).

III. RESULTS AND DISCUSSIONS

In Fig. 1, the powder XRD pattern of $EuCu_2Ge_2$ is shown, which is a characteristic of the $ThCr_2Si_2$-type crystal structure with the tetragonal space group $I4/mmm$ (No. 139). XRD pattern of $EuCu_2Ge_2$ shows it to be a single phase. No extra reflections were observed in the XRD pattern that would indicate the presence of Eu_2O_3 or the presence of any other impurity phases. Rietveld refinement of the XRD pattern was carried out using the FULLPROF package.[21] The background was fitted using linear interpolation between the data points. Pseudo-Voigt profile shape function was selected to model the line shapes of the various Bragg reflections. During the refinement scale factor, zero correction, shape parameters, half-width parameters, lattice parameters, positional coordinates, and isotropic thermal parameters were varied. Eu and Cu atoms occupy the fixed high-symmetry special positions while the position of Ge was varied. The Wyckoff positions of the different atoms are as follows: Eu:($2a$) 0, 0, 0; Cu:($4d$)

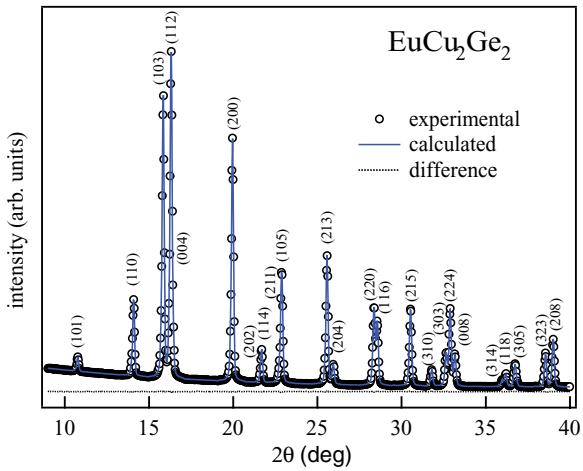

FIG. 1. (Color online) The x-ray diffraction pattern of the compound $EuCu_2Ge_2$ at 300 K. The experimental data are denoted by open circles, while the blue line through the circles represents the results of the Rietveld refinement. The lower dotted line represents the difference curve between experimental and calculated patterns.

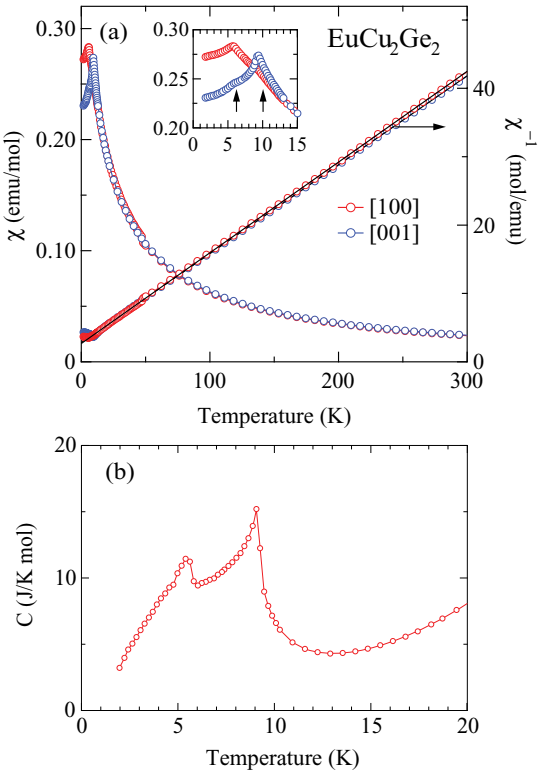

FIG. 2. (Color online) (a) Magnetic susceptibility (χ) of $EuCu_2Ge_2$ measured in the magnetic field of 3 KOe. Inset shows the zoomed region below 15 K. Arrows in the inset marked the antiferromagnetic transitions. Inverse χ is plotted on the right scale and solid line shows the fitting of the Curie-Weiss law. (b) Specific heat (C) of $EuCu_2Ge_2$ at low temperatures.

0, 0.5, 0.25; and Ge:(4*e*) 0, 0, 0.376. The lattice constants obtained from the Rietveld refinement are $a = 4.2117(4)$ Å and $c = 10.2236(4)$ Å and the unit cell volume $V = a^2c$ is 181.35 Å^3. These results are comparable with the reported lattice constants of polycrystalline $EuCu_2Ge_2$ ($a = 4.215$ Å, $c = 10.18$ Å, and $V = 180.9$ Å^3).[5]

The temperature dependence of the magnetic susceptibility (χ) of $EuCu_2Ge_2$ along the [100] and [001] directions are shown in Fig. 2(a). Inset in Fig. 2(a) shows the zoomed region below 15 K. Along the [001] direction $\chi(T)$ exhibits a broad peak at 6 K and a sharp peak at 9.2 K. The trend in $\chi(T)$ reverses along the [100] direction and a broad peak was observed at 9.2 K and a sharp peak at 6 K. The peaks in the $\chi(T)$ reveal the magnetic ordering of Eu magnetic moments at these temperatures. Thus there are two antiferromagnetic transitions observed at $T_{N1} = 6$ K and $T_{N2} = 9.2$ K in the single-crystal $EuCu_2Ge_2$ which is consistent with the previous reports.[4,22] Above 10 K, the inverse susceptibility (χ^{-1}) follows a Curie-Weiss law. The effective magnetic moment(μ_{eff}) and the paramagnetic Curie temperature (θ_p) along the [100] and [001] directions were determined from fitting the Curie-Weiss law to χ^{-1} as shown in Fig. 2(a). Along the [100] and [001] directions, the values of θ_p are -20 and -21 K whereas, μ_{eff} are 7.76 and 7.84 μ_B/Eu, respectively. The experimental values of μ_{eff} are slightly less than the theoretical value of 7.94 μ_B/Eu for divalent Eu ions. This may indicate the presence of a minor fraction of Eu^{3+} ions. The negative values of θ_p indicate the predominantly antiferromagnetic interaction between the Eu^{2+} magnetic moments. The temperature dependence of specific heat in Fig. 2(b) also reveals two peaks corresponding to two magnetic transitions at 9.2 and 6 K.

The VB spectra of $EuCu_2Ge_2$ recorded at photon energies from 134 to 170 eV are shown in Fig. 3. The background obtained by the Tougaard procedure[23] has been subtracted from raw data. A clear Fermi edge of the $EuCu_2Ge_2$ was observed. The VB is dominated with the Cu 3*d* states centered at -3.6 and -4 eV and a small peak at -1 eV corresponds to the Eu $4f$ states. As the incident photon energy is increased, features at -1.0 and -1.8 eV (marked as A and B in Fig. 3) become more prominent reaching a maximum at 140 eV. The feature A is attributed as the Eu^{2+} $4f$ state and the resonance phenomenon arises due to the quantum interference of direct photoemission and the Auger process. For the divalent transition, the direct photoemission phenomena is $4d^{10}4f^7 + h\nu \rightarrow 4d^{10}4f^6 + e$, and the photoionization of the excited electron into the conduction band followed by Auger emission is $4d^{10}4f^7 + h\nu \rightarrow 4d^9 4f^8 \rightarrow 4d^{10}4f^6 + e$. As the incident photon energy is further increased, the states at -3.6, -4, -7.3, and -11 eV (marked as C, D, E, and F in Fig. 3) showed an enhancement in intensity. This is quite evident in the contour plot shown in Fig. 4. Features C, D, E, and F start manifesting at 141 eV and show a maximum at 143 eV. These features also show a second resonance at 150 eV incident energy. It is well known for Eu compounds that the $4f^7 \rightarrow 4f^6$ spectral weight (divalent contribution) exists in the energy region 0 to 2 eV below E_F and the $4f^6 \rightarrow 4f^5$ spectral weight (trivalent contribution) exists at 3 to 12 eV below E_F.[24] It was observed that after $h\nu = 140$ eV, along with the $4f^6$ emission due to divalent Eu, there is also the contribution from $4f^5$ emission due to the trivalent Eu states in the VB (see Fig. 4).

The trivalent resonance photoemission phenomena for Eu is given as $4d^{10}4f^6(5d6s)^3 + h\nu \rightarrow 4d^9 4f^7(5d6s)^3 \rightarrow 4d^{10}4f^5(5d6s)^3 + e$. In order to obtain a divalent $4f^6$ final state with the onset of the trivalent state, there remain two possibilities: (1) an Auger decay via the ($5d6s$) states, i.e.,

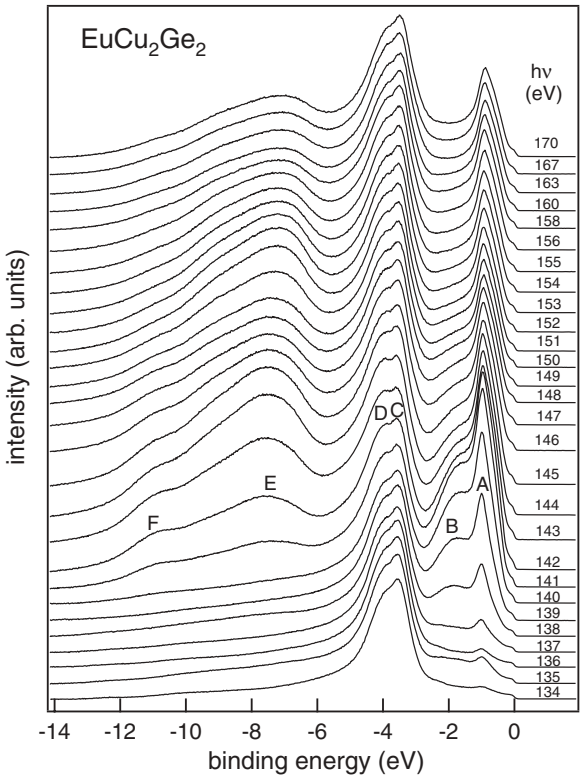

FIG. 3. Normal emission VB spectra of $EuCu_2Ge_2$ recorded at different photon energy across the Eu $4d$-$4f$ resonance.

$4d^{10}4f^6(5d6s)^2$ configuration, and (2) by the additional $4f$ screening of the trivalent state. Both the processes would be resonantly enhanced together with the $4f^5$ final-state photoemission signal from the trivalent Eu ion. Therefore the preceding onset of the $4f^6$ emission resonance clearly shows the initial state character of the divalent Eu surface emission.[24] The trivalent Eu $4f$ feature due to the $4d^{10}4f^5(5d6s)^3$ contribution is clearly observed at -7.3 eV (marked as E in Figs. 3 and 4) and the other contribution due to the $4d^{10}4f^6(5d6s)^2$ configuration or by the $4f$ screened state as observed at -3.6

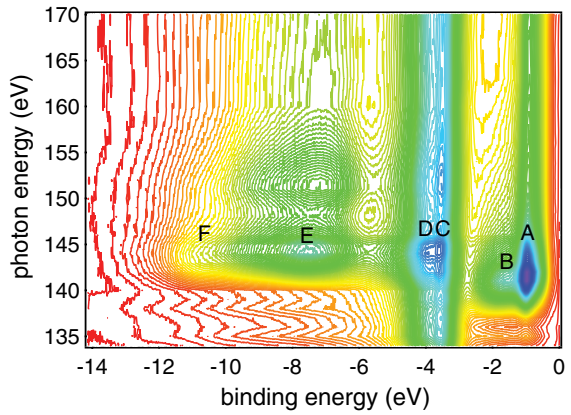

FIG. 4. (Color online) Contour plot as a function of incident photon energy vs the binding energy across the $4d$-$4f$ resonance for $EuCu_2Ge_2$. In the gray scale (rainbow for color), the lightest (red) contour corresponds to the minimum intensity and darkest (violet) contour corresponds to the maximum intensity.

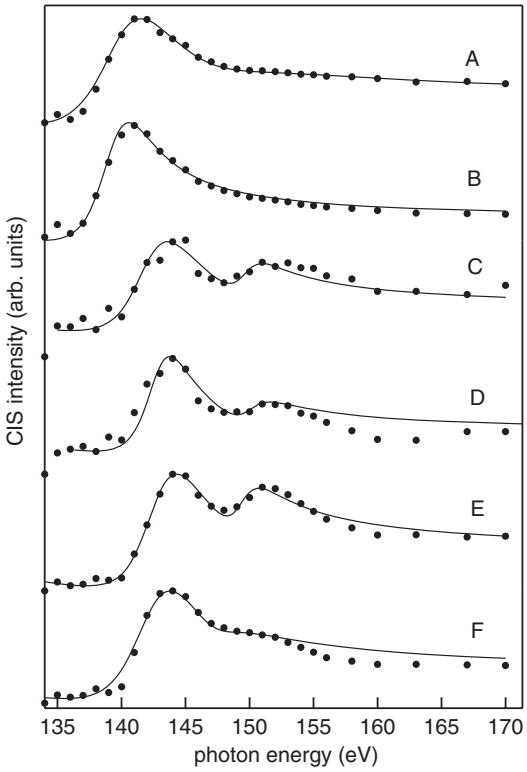

FIG. 5. The constant initial state of the resonant features A, B, C, D, E, and F as a function of incident photon energy. The solid line shows the fitting with the Fano line shape. For the clarity of presentation all the features are normalized to same height.

and -4 eV (marked by C and D in Figs. 3 and 4). The difference between Eu^{2+} and Eu^{3+} states in $EuCu_2Ge_2$ is about 6.3 eV. Similar difference in Eu^{2+} and Eu^{3+} states has been observed for other Eu based intermetallic systems like $EuPt_5$, $EuRh_2$, EuTe, and $EuCu_2(Ge_{1-x}Si_x)_2$.[7,24,25]

In Fig. 5, we show the constant initial state (CIS) intensities plotted for all the features from A to F as obtained in the VB spectra of $EuCu_2Ge_2$. The CIS intensity plots have been obtained from Fig. 3 by plotting the normalized intensity of the marked regions (A, B, C, D, E, and F) at fixed binding energy positions of the respective features. In the vicinity of the resonance process, CIS spectra have been shown to give rise to a characteristic Fano line profile[26] that originates from an interference between direct photoionization and indirect photoionization process. This leads to Fano profiles of the form $\sigma(h\nu) = \sigma_a \frac{(q+\epsilon)^2}{1+\epsilon^2} + \sigma_b$, with the reduced energy $\epsilon = (h\nu - E_0)/\Gamma$, where E_0 is the resonance energy, Γ is the half-width of the line or the natural width given by the decay rate of the autoionization resonance. The Fano parameter q, which is mainly the line profile index, represents the discrete/continuum mixing strength, i.e., the coupling strength. The cross sections σ_a and σ_b represent the nonresonant background cross sections for transitions to continuum states that interact or do not interact, respectively, with discrete autoionization states. Therefore σ_a is affected by the interaction whereas σ_b is constant. With $|i\rangle$, $|v\rangle$, and $|f\rangle$ describing the initial, intermediate (discrete state), and final continuum state, respectively, the linewidth can be written as $\Gamma = 2\pi |\langle f| V |v\rangle|^2$, where V represents the Coulomb

TABLE I. Fano line-shape fitting results for the valence band features of $EuCu_2Ge_2$. E_B denotes the binding energies of the features. Calculated values of the parameters q, Γ, and the resonance energy E_0 describing the Fano line shapes in the excitation spectra for the Eu $4d$-$4f$ resonance are listed.

Features	E_B (eV)	E_0 (eV)	q	Γ (eV)
A	1	139.85	2.13	3.89
B	1.8	139.35	2.14	2.6
C	3.6	142.24, 149.59	2.13, 0.99	3.11, 1.86
D	4	141.54, 148.59	2.35, 0.8	2.25, 2
E	7.3	142.85, 149.7	1.9, 0.98	3.19, 1.9
F	11	142.24, 147.29	1.96, 0.2	3.59, 2.8

interaction and $q = \frac{\langle v|r|i\rangle}{\pi\langle v|V|f\rangle\langle f|r|i\rangle}$, which represents the ratio of the dipole matrix element of a transition to a discrete state to that of a transition to the continuum, which interacts with the discrete state. If the coupling strength between the final state $|f\rangle$ and the discrete state $|v\rangle$ is very weak, the value for q becomes large and a Lorentz line shape is observed in the cross section; for a strong coupling strength, q is close to zero and one can see a window dip; for all other cases of the coupling strength, the variation in the cross section caused by a resonance is described by a Fano-like line shape. If q is negative, the minimum in the absorption cross section occurs on the high-energy side of the line and otherwise on the low-energy side. In Fig. 5, the markers (filled circles) and the solid line show the experimental data points and the fitted Fano line shape, respectively, achieved with a curve of the form $(q+\epsilon)^2/(1+\epsilon^2)$. Here, we have not calculated the Coulomb potential and the dipole matrix elements but the determined Γ and q values, which appear to be reasonable when compared to the values previously reported for $CeAg_2Ge_2$.[27] The parameters obtained from the fitting are listed in Table I. Features A and B corresponds to purely Eu^{2+} state, while the features C, D, E, and F are related to the Eu^{3+} states. Interestingly, the multiplet structure has been observed for the Eu^{3+} state (feature C, D, E, and F in Fig. 5) with the main components ascribed to the $^6H_{5/2}$ and $^6F_{5/2}$ terms at nearly 143 and 150 eV, respectively. Similar features have been observed for the EuF_3.[28] To fit both the features we have used two Fano line shapes and the results are listed in Table I. Eu resonance profile in $EuCu_2Ge_2$ shows the different Fano line shapes for Eu^{2+} and Eu^{3+} states because these are two different Eu $4f$ states and the overlap of these states with the conduction bands, or the degree of hybridization is different for both the states.

To facilitate the interpretation of the experimental results, we carried out density of states (DOS) calculations using the GGA and GGA + U methods, where the U refers to the onsite Coulomb energy in an open $4f$ shell. We have also included the SO coupling for the Eu $4f$ shells. The GGA calculation with the SO interaction is shown in Fig. 6(a), for $EuCu_2Ge_2$. The total DOS shows enhancement near E_F due to the Eu $4f$ states. The DOS centered at -3.0 eV is mainly due to the Cu states and the DOS near -10 eV is mainly due to the Ge states. The features around -1.5 and -4 eV show the hybridization between Cu and Ge states. We find that the GGA calculation without considering the correlation effect does not show the

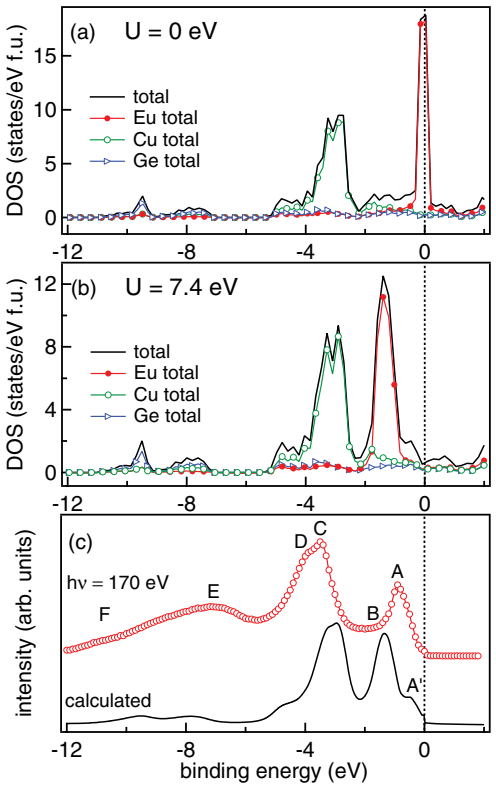

FIG. 6. (Color online) Total DOS, Eu total, Cu total and Ge total DOS calculated by (a) GGA method and (b) GGA + U method. (c) shows the calculated VB (with GGA + U method) compared with the experimental VB at 170 eV.

features matching with the experimental VB spectra as a large DOS related to Eu $4f$ states was observed near E_F in the calculation which is not present in the experimental data. To account for correlation effects in the open atomic-like $4f$ shell, we have performed the GGA + U calculations, where U in the $4f$ shell was set to 7.4 eV for Eu and is shown in Fig. 6(b). The features at -3, -4, and -10 eV are very much similar to the DOS calculation without considering U [see Figs. 6(a) and 6(b)]. The only difference is in the Eu $4f$ states that move sizeably away from the Fermi level and appear at -1.39 eV [see Fig. 6(b)] when U is included. This Eu $4f$ related feature also shows a small hybridization with the Cu and Ge states. The total DOS in Fig. 6 is the sum of partial DOS of Eu, Cu, and Ge as shown in Fig. 7. The comparison of the experimental VB at 170 eV and the calculated VB obtained from broadened DOS is shown in Fig. 6(c). To broaden the DOS, we have added the PDOS of Eu, Cu, and Ge as shown in Fig. 7 after multiplying it with the photoionization cross sections at 170 eV.[29] This added DOS is then multiplied with the Fermi function at the measurement temperature and convoluted with a Voigt function. The full width at half maximum (FWHM) of the Gaussian component is taken to be 0.02 eV of the Voigt function, which represents the instrumental resolution in the photoemission measurement. The energy-dependent Lorentzian FWHM that represents the life-time broadening is 0.05E, where E is the energy with respect to E_F.[30,31] The inelastic background and the matrix elements are not considered. This is a standard procedure for comparing the

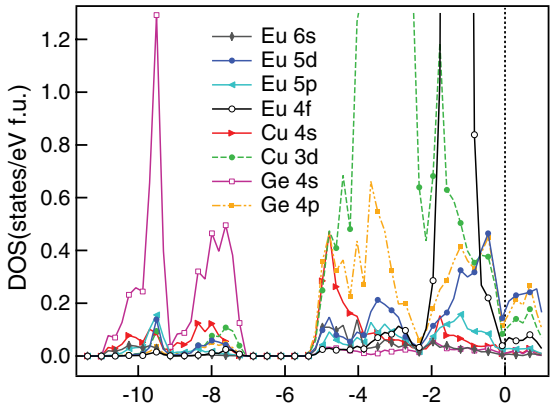

FIG. 7. (Color online) PDOS of Eu, Cu, and Ge calculated by using GGA + U method.

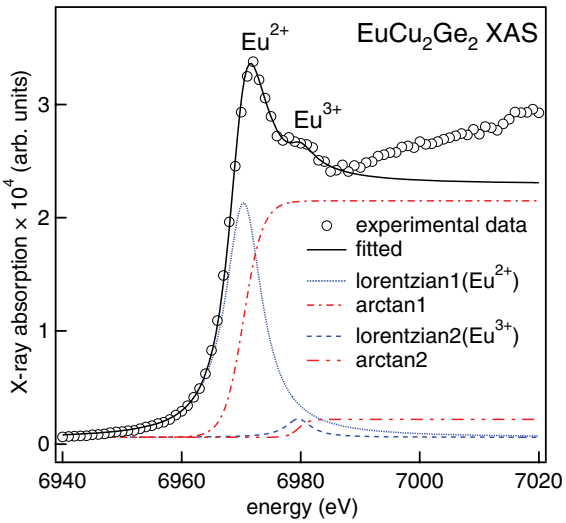

FIG. 8. (Color online) L_3 x-ray absorption edge of Eu in $EuCu_2Ge_2$ at room temperature. Solid line is fitted data with two components arctangent step function (red dot dash lines) with Lorentzian (blue dashed lines).

photoemission spectrum with the calculated DOS.[27,30] We observe that the calculated VB with GGA + U method is comparable with the experimental spectra [see Fig. 6(c)] at the off-resonance ($h\nu = 170$ eV) energy implying that the electron-electron correlation plays a major role in this system. There are small differences between the experiment and the theoretical calculation like the position of the feature A and C that could be related to the fact that the DFT is a ground-state calculation and it does not take into account the sample related effects such as the presence of antisite defects and site disorder, etc. Moreover, another feature marked by A′ for the calculated VB in Fig. 6(c), which shows a lesser intensity in the experimental spectra. Similar kind of discrepancy between the experimental and the theoretical calculation has been observed for Heusler systems like Ni_2MnGa[32] and the possible reason is due to the presence of site disorder or antisite defects in the system.

In Fig. 7, we show the partial DOS (PDOS) of Eu 4f, Eu 5p, Eu 5d, Eu 6s, Cu 3d, Cu 4s, Ge 4s and Ge 4p obtained from the GGA + U calculation. The states very near to the E_F at −0.45 eV are the hybridized Eu 5d, Eu 4f, Ge 4p, and Cu 3d states. These states mainly contribute to the conduction band. The states at −1.39 eV are dominated by the Eu 4f states and also shows a small hybridization with the Cu 3d, Ge 4p, and Eu 5d and 5p states. The features centered at around −3 eV are dominated with the Cu 3d states. These Cu 3d states shows hybridization with the Ge 4p states and the Eu 4f and 5d states at −3.5 and −4.8 eV. The DOS centered at −8 and −9.5 eV are mainly dominated with the Ge 4s states with a small hybridization with the Cu 3d, Cu 4s, and Eu 5d states. In addition to this, −9.5 eV feature also show a hybridization with the Eu 5p states.

The DOS calculations give the information of only the atomic Eu 4f states, it doesn't tells about the ionic states in the system. The DOS calculations were done by taking the ideal ordered structure of $EuCu_2Ge_2$ and the stable ground state of Eu in this system is Eu^{2+} and not the Eu^{3+}. Hence in the DOS calculations in Fig. 7, we do not observe an enhanced Eu 4f DOS at −7.3 eV (feature E) corresponding to Eu^{3+} as observed for Eu 4f state at −1 eV (feature A) corresponding to Eu^{2+} state. Rather, we observe a very small PDOS of Eu 4f state at −7.3 eV. If Eu^{3+} state were a stable state in this system, we would expect a enhanced DOS at feature E, which we don't see. Hence although the Eu 4f states shows the hybridization with the Cu 3d and Ge 4p states but the dominance of the states in the DOS clearly shows the stable ionic configuration. Here, we find the Eu^{2+} state is more stable state in $EuCu_2Ge_2$.

In order to see whether the mixed valence in $EuCu_2Ge_2$ is a surface or a bulk property, we have carried out L_3 x-ray absorption edge measurements in fluorosence mode and the result is shown in Fig. 8. The L_3-absorption edge corresponds to the transition of an electron from $2p_{3/2}$ core level to unfilled levels near the Fermi level and differs for the two valence states. The relative intensities and the position of the Eu^{2+} and Eu^{3+} states were determined by fitting the XAS spectra with a two-component model consisting of an arctangent step function and a Lorentzian peak for each valence state. Arctangent is an *ad hoc* step function for representing the transition to the continuum states. The constraint used in the fitting was that the threshold energy for both the Lorentzian peak and the step function for a given valence state was kept the same. Hence, the threshold energy of the Eu^{2+} and Eu^{3+} states were determined to be 6970.4 nd 6979.6 eV, respectively. The difference between the Eu^{2+} and Eu^{3+} states is larger in XAS (9.2 eV) than the difference determined from RPES (6.3 eV). This is because XAS does not provide the direct information about the valence 4f states of the Eu atoms. In photoemission when a positively charged core hole is created by innershell excitation, nearby electron orbitals screen the core hole and are pulled inward reducing the magnitude of the measured binding energy by an amount equal to the relaxation energy. So when the excited electron leaves the solid, the measured relaxation energies are few electron volts. However, in XAS, the core electron that receives the energy just slightly in excess of the threshold value remains in the vicinity of core hole and the screening effect of its negative charge reduces the relaxation energy. Hence relaxation and screening effects are less in XAS than in photoemission which gives the difference in determining the Eu^{2+} and Eu^{3+} states from both

the techniques. The solid line in Fig. 8 shows the total fit to the experimental data (open circles). The two components are shown by different types of broken lines. This type of fitting is often used for the analysis of the mixed valence state in rare earth intermetallic compounds like, for example, $Sm_{1-x}Gd_xS$ and $Eu_{0.95}Fe_4Sb_{12}$.[33,34] Hence from fitting the valence state population for Eu^{2+} state is about 92% and Eu^{3+} state is about 8%. However, the percentage of Eu^{3+} state determined from XAS is about 5–6% higher than the susceptibility measurement and similar difference in the determination of the ratio of Eu states has been observed for EuS.[35] From XAS measurements on $EuCu_2Ge_2$, Fukuda *et al.*[6] also observed the presence of small quantity of Eu^{3+} state in the system which was not observed by the other bulk measurements. However, the Eu absorption edge and the photoemission measurements are in striking contrast to the observations from the Mössbauer experiments where only divalent Eu state is reported.[4] Similar discrepancy has been observed for other Eu based systems like the $EuRh_2P_2$, $EuPd_2P_2$, $Eu_{0.83}Fe_4Sb_{12}$, etc., where Mössbauer shows a single line characteristic of stable Eu^{2+} state but the L_3 edge shows a very pronounced double-peak structure characteristic of Eu^{2+} and Eu^{3+} states.[8–10]

Valence fluctuation in this system is ruled out since we do not observe any Eu $4f$ states in the vicinity of E_F in the RPES data that are supported by the DOS calculations. Moreover the energy separation (ΔE) of the absorption maxima corresponding to the Eu^{2+} and Eu^{3+} states is reported to be less than 8 eV for the valence fluctuating systems.[36–39] For $EuCu_2Ge_2$, $\Delta E \approx 9.2$ eV, which indicates that $EuCu_2Ge_2$ is certainly not a valence fluctuating system.[9] Therefore we predict that $EuCu_2Ge_2$ system is a inhomogeneous static mixed valence system.[11] The static mixed valency may can come from the inhomogeneity or the site disorders in the system. In particular, XAS indicates a minor (8 %) fraction of europium Eu^{3+} ions in $EuCu_2Ge_2$. The amount of this minor disorder may also depend upon sample preparation conditions and annealing treatment. It is certainly small enough in the sample on which Mössbauer was done that it escaped detection. The effect of near-neighbor environment on the valence state of Eu ions in $EuPd_2Si_2$, $EuCu_2Si_2$, $EuNi_2Si_2$, and $EuPd_3B$, is well documented.[36,39] The VB photoemission spectra at the off-resonance do not give any signature of the trivalent state (see 134 eV spectra in Fig. 3) because the photoionization cross section of trivalent state is much smaller than the divalent state. This may be the reason why Hossain *et al.* didn't get any signature of the trivalent state in the XPS valence band.[7] We have also obtained similar XPS results (not shown in the paper) as obtained by Hossain *et al.*[7] They have observed a weak broad feature at 8 eV from the E_F and interpreted it as a plasmon loss structure. From our calculation, the feature at -8 eV represents the hybridized Ge, Cu, and Eu states (see Figs. 6 and 7). The signature of trivalent state was obtained only when the photon energy was scanned across the trivalent resonance energy. Moreover, our theoretical calculation also doesn't show the mixed valence state because it doesn't take into account the antisite defects or disorders in the system. We therefore feel that the valence mixing in the $EuCu_2Ge_2$ is inhomogeneous and static may be induced by the disorders or the near-neighbor environment of Eu.

IV. CONCLUSION

In this paper, we have performed the RPES study on $EuCu_2Ge_2$ across the Eu $4d$-$4f$ resonance. VB of $EuCu_2Ge_2$ shows two resonance features due to Eu^{2+} and Eu^{3+} states which can be fitted with Fano line shape profile and the resonance energies estimated are 140 and 143 eV for Eu^{2+} and Eu^{3+} states, respectively. The Eu $4f$ atomic-like correlation effect is playing a major role in this system and is explained with the theoretical GGA + U calculations. The Eu $4f$ related resonant features are found to be hybridized with the Cu and Ge states. XAS spectra also show the evidence of both the states. While the bulk europium ions are in the divalent state in $EuCu_2Ge_2$, the remaining small fraction of Eu^{3+} ions are tentatively attributed to minor atomic disorder or the near neighbor environment of Eu.

ACKNOWLEDGMENTS

The authors wish to thank P. D. Gupta, P. Chaddah, and Tapas Ganguli for their constant encouragement and support. D. M. Phase is thanked for providing the experimental support.

*soma@rrcat.gov.in

[1] E. R. Bauminger, D. Froindlich, I. Nowik, S. Ofer, I. Felner, and I. Mayer, Phys. Rev. Lett. **30**, 1053 (1973).

[2] T. K. Hatwar, R. M. Nayak, B. D. Padalia, M. N. Ghatikar, E. V. Sapathkumaran, L. C. Gupta, and R. Vijayaraghavan, Solid State Commun. **34**, 617 (1980); E. V. Sapathkumaran, L. C. Gupta, R. Vijayaraghavan, K. V. Gopalakrishnan, R. G. Pillay, and H. G. Devare, J. Phys. C **14**, L237 (1981).

[3] H.-J. Hesse, R. Lübbers, M. Winzenick, H. W. Neuling, and G. Wortmann, J. Alloys Compd. **246**, 220 (1997).

[4] P. Wang, Z. M. Stadnik, J. Ukrowski, B. K. Cho, and J. Y. Kim, Solid State Commun. **150**, 2168 (2010).

[5] I. Felner and I. Nowik, J. Phys. Chem. Solids **39**, 767 (1978).

[6] S. Fukuda, Y. Nakanuma, J. Sakurai, A. Mitsuda, Y. Isikawa, F. Ishikawa, T. Goto, and T. Yamamoto, J. Phys. Soc. Jpn. **72**, 3189 (2003).

[7] Z. Hossain, C. Geibel, N. Senthilkumaran, M. Deppe, M. Baenitz, F. Schiller, and S. L. Molodtsov, Phys. Rev. B. **69**, 014422 (2004).

[8] E. V. Sampathkumaran, B. Perscheid, W. Krone, and G. Kaindl, J. Magn. Magn. Mater. **47–48**, 407 (1985).

[9] A. Grytsiv, P. Rogl, St. Berger, Ch. Paul, E. Bauer, C. Godart, B. Ni, M. M. Abd-Elmeguid, A. Saccone, R. Ferro, and D. Kaczorowski, Phys. Rev. B. **66**, 094411 (2002).

[10] G. Michels, M. Roepke, T. Niemöller, M. Chefki, M. M. Abd-Elmeguid, H. Micklitz, E. Holland-Moritz, W. Schlabitz, C. Huhnt, B. Büchner, A. Wurth, A. Mewis, and V. Kataev, J. Phys.: Condens. Matter **8**, 4055 (1996).

[11]C. Felser, S. Cramm, D. Johrendt, A. Mewis, O. Jepsen, G. Hohlneicher, W. Eberhardt, and O. K. Andersen, Europhys. Lett. **40**, 85 (1997).
[12]A. K. Sinha, A. Sagdeo, P. Gupta, A. Kumar, M. N. Singh, R. K. Gupta, S. R. Kane, and S. K. Deb, AIP Conf. Proc. **1349**, 503 (2011).
[13]Soma Banik, S. K. Deb, D. M. Phase, and A. Thamizhavel, AIP Conf. Proc. **1349**, 811 (2011).
[14]F. Polack, M. G. Silly, C. Chauvet, B. Lagarde, N. Bergeard, M. Izquierdo, O. Chubar, D. Krizmancic, M. Ribbens, J. P. Duval, C. Basset, S. Kubsky, and F. Sirotti, AIP Conf. Proc. No. 1234 (AIP, New York, 2010), p. 185.
[15]P. Hohenberg and W. Kohn, Phys. Rev. B **136**, 864 (1964); W. Kohn and L. J. Sham, *ibid*. **140**, 1133 (1965).
[16]P. Blaha, G. Schwarz, D. Madsen, K. Kvasnika, and J. Luitz, WIEN2K, Technical Universitt Wien, Austria (2001).
[17]D. Singh and L. Nordstrm, *Plane waves, pseudopotentials and the LAPW method*, 2nd ed. (Springer, New York, 2006).
[18]E. Sjostedt, L. Nordstrom, and D. J. Singh, Solid State Commun. **114**, 15 (2000).
[19]J. P. Perdew, K. Burke, and M. Ernzerhof, Phys. Rev. Lett. **77**, 3865 (1996); J. P. Perdew, K. Burke, and Y. Wang, Phys. Rev. B **54**, 16533 (1996).
[20]P. Larson, W. R. L. Lambrecht, A. Chantis, and M. van Schilfgaarde, Phys. Rev. B **75**, 045114 (2007).
[21]Rodiguez J. Carvajal, FULLPROF, Laboratoire Leon Brillouin (CEA-CNRS), France.
[22]Z. Hossain, C. Geibel, H. Q. Yuan, and G. Sparn, J. Phys.: Condens. Matter **15**, 3307 (2003).
[23]S. Tougaard, Surf. Sci. **216**, 343 (1989).
[24]W. D. Schneider, C. Laubschat, G. Kalkowski, J. Haase, and A. Puschmann, Phys. Rev. B **28**, 2017 (1983).
[25]K. Mimura *et al*., Physica B **351**, 292 (2004); B. A. Orlowski, B. J. Kowalski, M. Pietrzyk, and R. Buczko, Acta Phys. Pol. A **114**, S-103 (2008).
[26]U. Fano, Phys. Rev. **124**, 1866 (1961).
[27]Soma Banik, Aparna Chakrabarti, Devang A. Joshi, A. Thamizhavel, D. M. Phase, S. K. Dhar, and S. K. Deb, Phys. Rev. B **82**, 113107 (2010).
[28]J. Szade *et al*., Surf. Sci. **602**, 1525 (2008).
[29]J. J. Yeh and I. Lindau, At. Data Nucl. Data Tables **32**, 1 (1985).
[30]D. D. Sarma, N. Shanthi, S. R. Barman, N. Hamada, H. Sawada, and K. Terakura, Phys. Rev. Lett. **75**, 1126 (1995); Atsushi Fujimori and Fujio Minami, Phys. Rev. B **30**, 957 (1984).
[31]B. Reihl, T. Riesterer, J. G. Bednorz, and K. A. Müller, Phys. Rev. B. **35**, 8804 (1987).
[32]Aparna Chakrabarti, C. Biswas, S. Banik, R. S. Dhaka, A. K. Shukla, and S. R. Barman, Phys. Rev. B **72**, 073103 (2005).
[33]C. Godart, J. C. Achard, G. Krill, and M. F. Ravet-Krill, J. Less-Common Met. **94**, 177 (1983).
[34]V. V. Krishnamurthy, D. J. Keavney, D. Haskel, J. C. Lang, G. Srajer, B. C. Sales, D. G. Mandrus, and J. L. Robertson, Phys. Rev. B. **79**, 014426 (2009).
[35]R. S. Selinsky, D. J. Keavney, M. J. Bierman, and S. Jin, Appl. Phys. Lett. **95**, 202501 (2009).
[36]B. Darshan, B. D. Padalia, R. Nagarajan, S. K. Dhar, S. K. Malik, and R. Vijayaraghavan, Phys. Rev. B **30**, 4031 (1984).
[37]A. Mitsuda, H. Wada, M. Shiga, and T. Tanaka, J. Phys.: Condens. Matter **12**, 5287 (2000).
[38]E. Kemly, M. Croft, V. Murgai, L. C. Gupta, C. Godart, R. D. Parks, and C. V. Segre, J. Magn. Magn. Mater. **47**, 403 (1985).
[39]Sujata Patil, R. Nagarajan, C. Godart, J. P. Kappler, L. C. Gupta, B. D. Padalia, and R. Vijayaraghavan, Phys. Rev. B. **47**, 8794 (1993).